Supporting Information

Experimental Procedures

Materials

Potassium bicarbonate (KHCO$_3$, Rhawn, AR, 99.5%), multi-walled carbon tubes (CNT, Sigma-Aldrich, 50-90 nm diameter, >95% carbon basis), metal phthalocyanine (MPc, M = Mg, Mn, Fe, Co, Ni, Cu, Zn, Sn, Aladdin, >95%,), Nafion 117 perfluorinated resin solution（~5% in a mixture of lower aliphatic alcohols and water, Rhawn), Ethanol (C_2H_5OH, Chemical Reagent, AR) and N, N-dimethylformamide (DMF, Chemical Reagent, AR). All solutions were prepared in ultrapure water (specific conductivity 18.2 MΩ cm^{-1}). High-purity argon gas (99.999%), high-purity carbon dioxide gas (99.999%), and synthetic air (21% O_2, 79% N_2) were from Harbin Qinghua Industrial Gases. The cation-exchange membrane used in this experiment is the Nafion 117 membrane provided by Du Pont Company.

Synthesis of catalysts:

10 mg of MPc (M = Mg, Mn, Fe, Co, Ni, Cu, Zn, Sn) (for a comprehensive overview, please refer to the periodic table (Fig. S1)) were dissolved in 30 mL of DMF solution. This was followed by 30 minutes of sonication. Subsequently, 100 mg of CNT was added to the solution. Following a 48-hour stirring period at room temperature, the solution was filtered and dried, and the resulting material was collected to yield the MPc/CNT powder.

Preparation of Electrodes

A solution of 0.5 mg of MPc/CNT catalyst in 1 mL of dispersion solution was prepared and sonicated until the solution was well dispersed. The resulting solution was then uniformly brushed onto the 1 cm×1 cm hydrophobic carbon paper, which

was subsequently dried in the water bath. The loading amount of the catalyst was approximately 0.5 mg/cm^2 .

Characterization

The samples were observed by Scanning Electron Microscopy (SEM) (EM-30plus) and Transmission Electron Microscope (TEM) (JEM-2100) to observe the morphology of the catalysts. The samples were analyzed spectroscopically using X-ray Diffractometer (XRD) (HZL10004), Raman Spectroscopy (DXR2), and Fourier Transform Infrared Spectroscopy (FT-IR) (Spectrum 400). X-ray photoelectron spectroscopy (XPS) (ESCALAB 250 XI+) was used for the determination of the surface chemical composition of the different catalytic materials.

Electrochemical Tests

Electrochemical tests were conducted using the three-electrode system. The catalyst was coated with hydrophobic carbon paper, serving as the working electrode. We utilized the Ag/AgCl electrode as the reference electrode, while the platinum mesh acted as the counter electrode. All electrochemical experiments were performed in the three-compartment sealed H-type electrolytic cell, separated by Nafion 117 membrane. All measurements were conducted using the electrochemical workstation (CHI 760E). The recorded potentials were subsequently converted to Reversible Hydrogen Electrode (RHE) potentials following the Nernst equation.

$$E_{RHE} = E_{Ag/AgCl} + 0.198 + 0.0592 \times pH$$

The Faraday efficiency was calculated in accordance with the following equation: $FE = \frac{ZnF}{Q}$ where Z represents the number of electrons transferred (for example, CO_2 reduction to CO, Z = 2), n denotes the number of moles of product, F is the Faraday constant (96485 C mol^{-1}) and Q is the charge.

The electrochemical tests were conducted in the CO_2-saturated 0.5 M $KHCO_3$ electrolyte, and the resulting products were analyzed making use of gas chromatography (GC, Agilent 8890). The gaseous products were identified as the CO and H_2. Subsequent analysis using the Liquid Chromatography (GC,

Agilent 1200) demonstrated that no liquid products were generated. The current densities at varying reaction potentials were evaluated at 25 ℃, and the products at each fixed potential were quantified. The gas products were collected online at 20-minute intervals through GC. The GC was employed for the detection of CO and CH_4, utilizing the Flame Ionization Detector (FID) and the Thermal Conductivity Detector (TCD) for the analysis of H_2, N_2, and other gases. The CO_2 flow rate at the inlet of the H cell was regulated at 20 mL/min using a standard series mass flow controller (ACU10FD-LC).

In suit IR

To investigate the reaction mechanism, we chose the Reflection Surface-Enhanced Infrared Absorption Spectroscopy (TR-SEIRAS) (WQF-530A). Our test setup was designed to emulate an H-type electrolytic cell, comprising an Ag/AgCl electrode as the reference electrode and a platinum sheet as the counter electrode. We recorded the real-time spectra at varying potentials in CO_2-saturated 0.5 M $KHCO_3$ electrolytes to observe the change in the reaction intermediates.

DFT

The reported calculations were performed using the Vienna ab initio simulation package (VASP) based on density functional theory (DFT)[1,2]. Meanwhile, the projector augmented wave (PAW) method was introduced to characterize the ion-electron interaction[3,4]. The exchange-correlation energy was described within the generalized gradient approximation (GGA) using Perdew–Burke–Ernzerhof (PBE) functional[5]. To deal with van der Waals interaction, Grimme's DFT-D3 method with Becke-Jonson damping was carried out[6,7]. The plane-wave energy cutoff of 450 eV and 1×1×1 gamma *k*-point grid were adopted to optimize the geometric structure. All atoms were determined to completely relax until the thresholds of energy and force convergence reached 10^{-6} eV and 0.02 eV $Å^{-1}$, respectively. For the CO_2RR process, the computational hydrogen electrode (CHE) model[8] suggested by Nørskov and co-workers was introduced to explain the proton-coupled electron transfer. In each elementary step, the Gibbs free energy change was defined as

$$\Delta G = \Delta E + E_{ZPE} - T S + \int C_p dT ,$$

where ΔE and ΔE_{ZPE} are the changes of total and zero point energy of the system, T is set to 298.15 K, ΔS denotes the entropy change, and the C_p is heat capacity. The adsorption energy of CO_2 ($E_{ads\text{-}CO2}$) was obtained by the equation:

$$E_{ads-CO_2} = E(*CO_2) - E(CO_2) - E(*) ,$$

where the $E(*CO_2)$ defines the total energy of the adsorption complex, $E(CO_2)$ and $E(*)$ denotes the isolated CO_2 molecule and catalyst, respectively.

Previous studies have shown that, in most cases, the solvation effect had little effect on the energy trend[9,10], thus the solvation effect was not considered in this paper.

Supplementary Figures

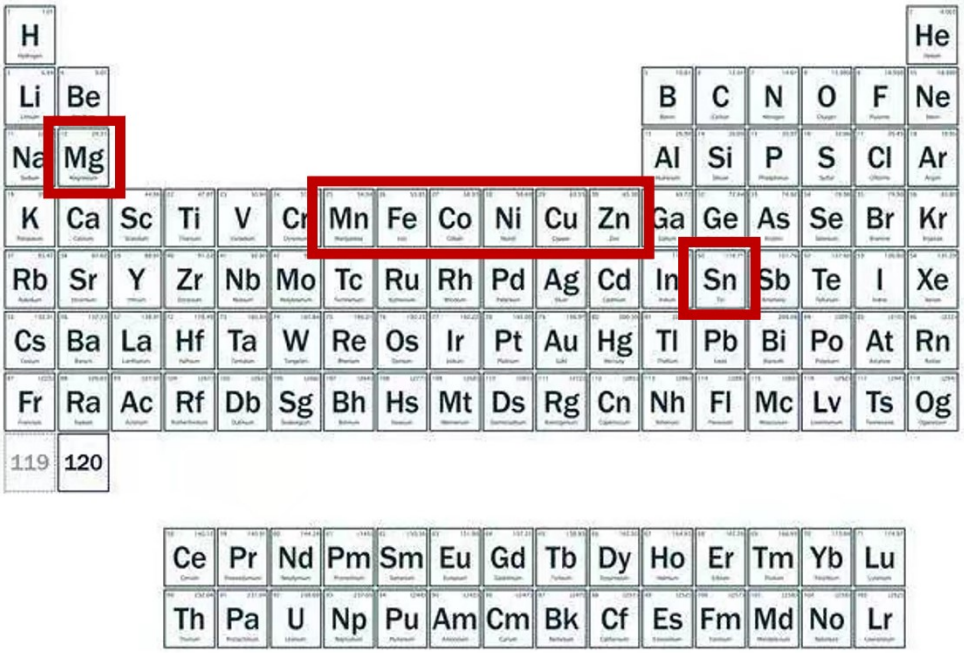

Figure. S1 Periodic table of the elements.

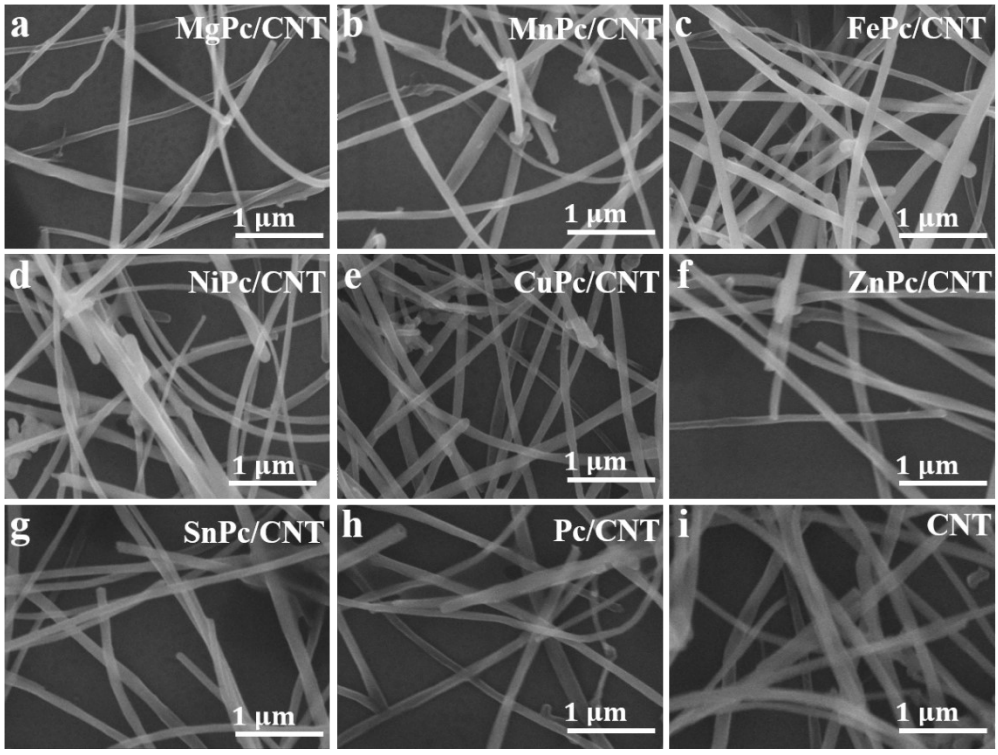

Figure. S2 SEM image of MPc/CNT (M = Mg, Mn, Fe, Ni, Cu, Zn, Sn), PC/CNT and CNTat 1 µm scale.

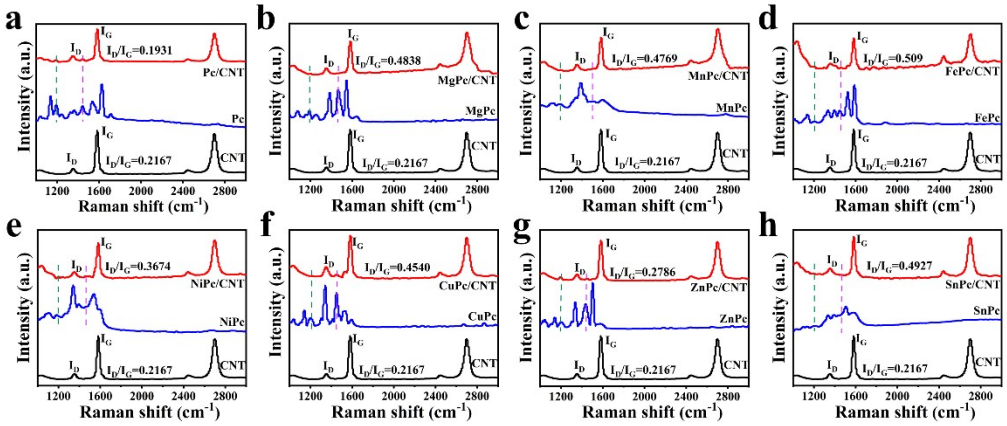

Figure. S3 Raman of MPc/CNT, MPc (M = Mg, Mn, Fe, Ni, Cu, Zn, Sn), PC/CNT, Pc and CNT.

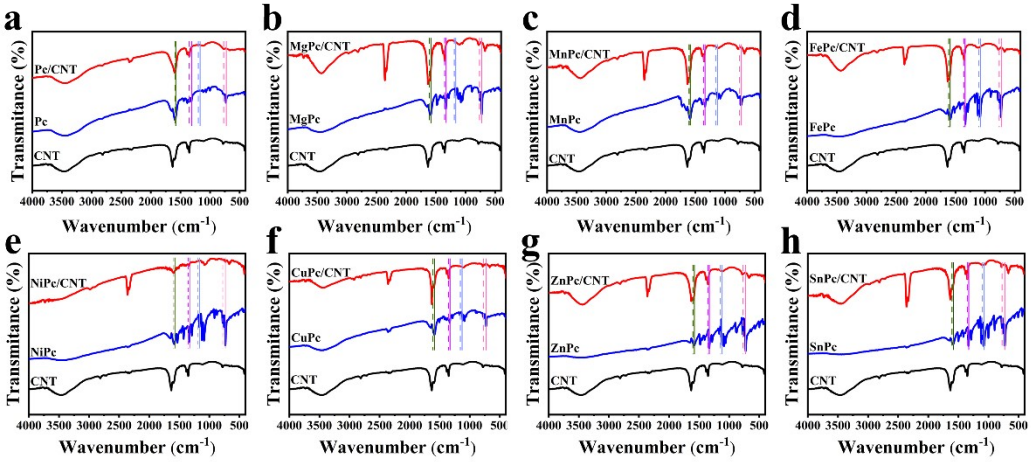

Figure. S4 FTIR of MPc/CNT, MPc (M = Mg, Mn, Fe, Ni, Cu, Zn, Sn), PC/CNT, Pc and CNT.

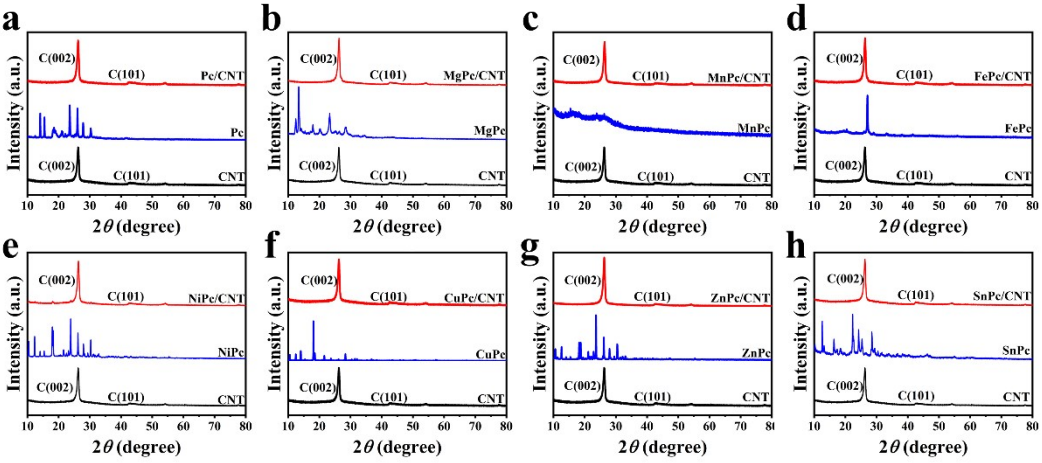

.

Figure. S5 XRD of MPc/CNT, MPc and CNT (M = Mg, Mn, Fe, Ni, Cu, Zn, Sn), PC/CNT, Pc and CNT.

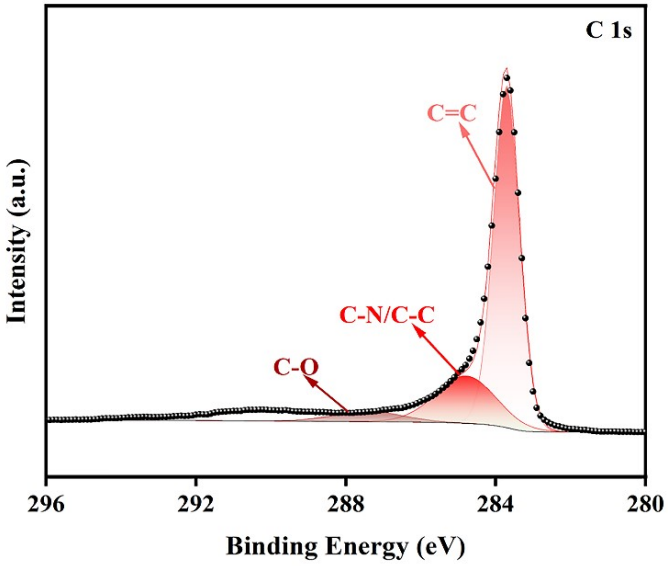

Figure. S6 XPS C spectrum of CoPc/CNT.

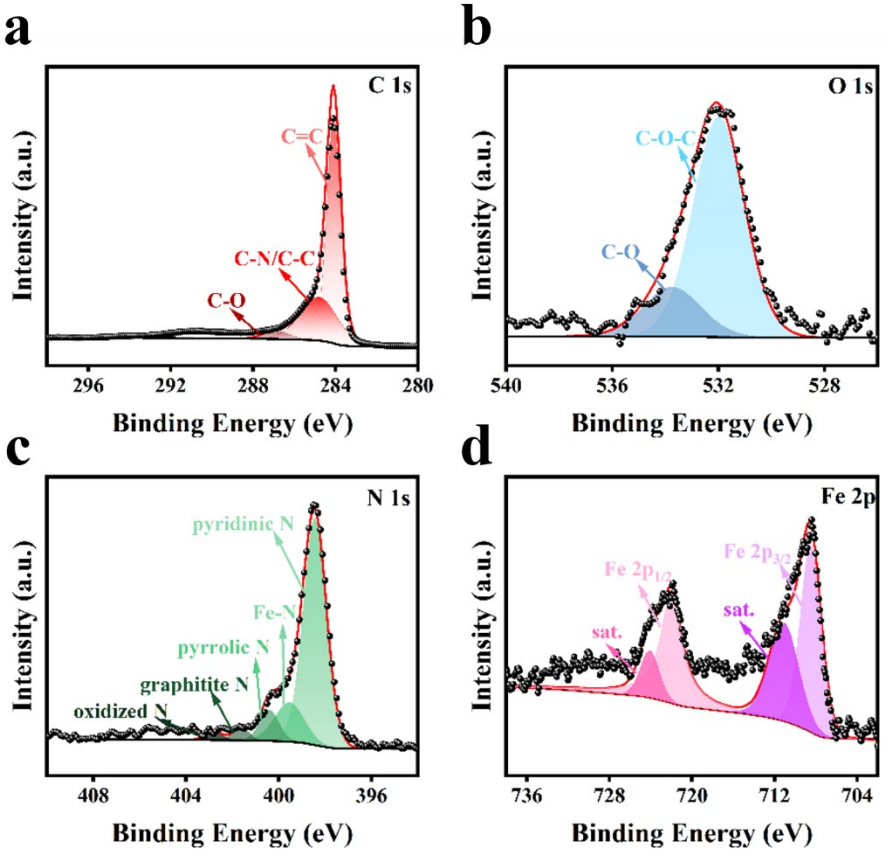

Figure. S7 XPS C 1s, O 1s, N 1s, Fe 2p spectrum of FePc/CNT.

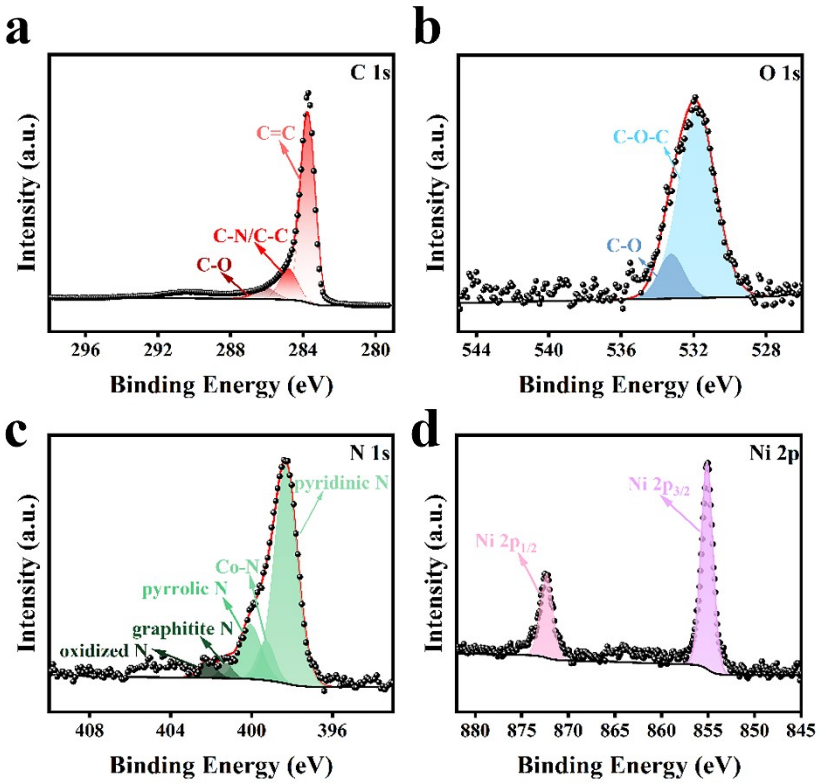

Figure. S8 XPS C 1s, O 1s, N 1s, Ni 2p spectrum of NiPc/CNT.

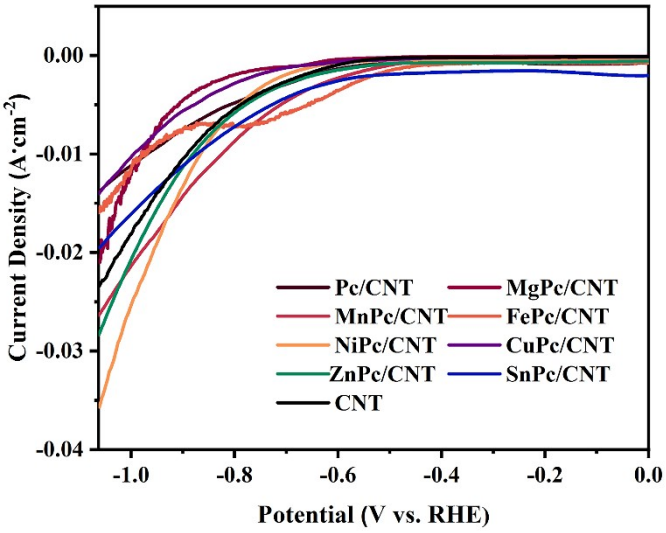

Figure. S9 LSV image of MPc/CNT (M = Mg, Mn, Fe, Ni, Cu, Zn, Sn), Pc/CNT and CNT.

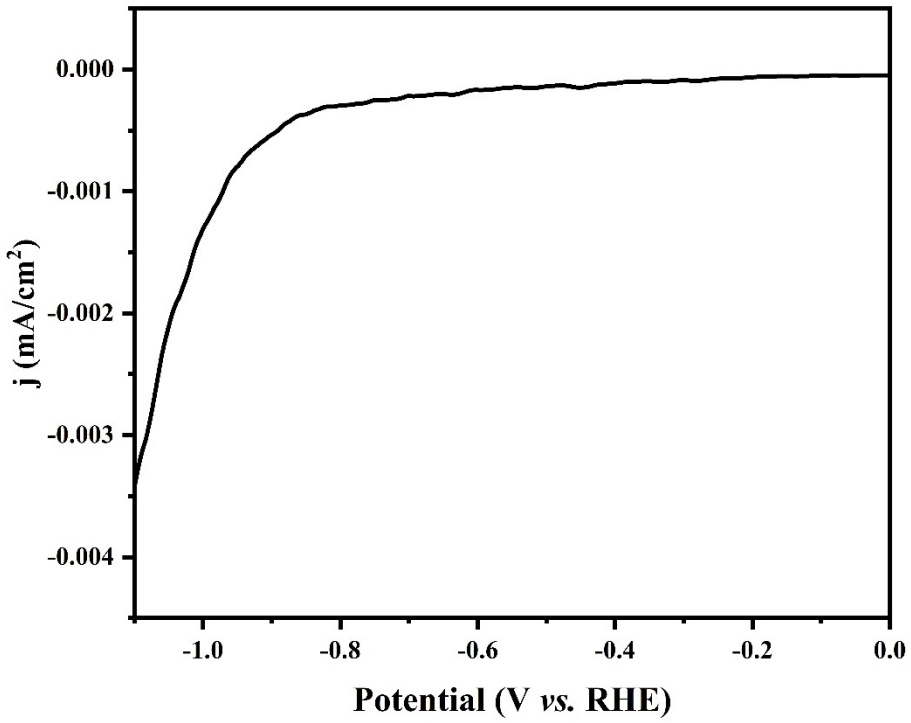

Figure. S10 LSV image of carbon paper.

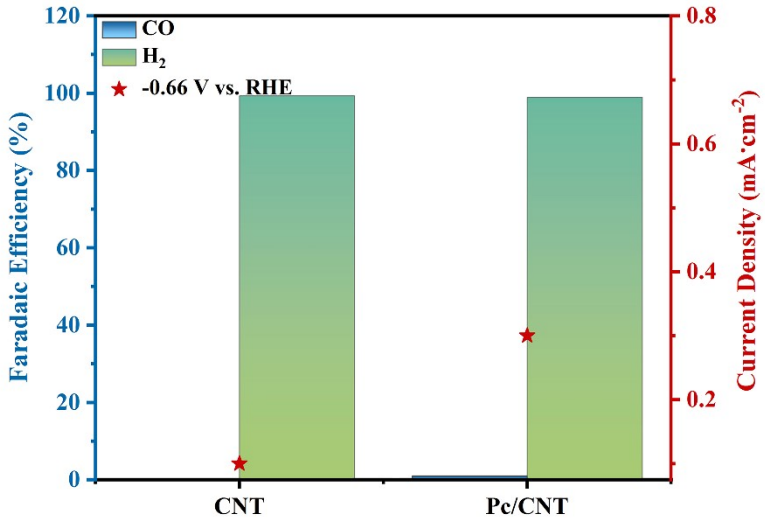

Figure. S11 FE_{CO} and current density image of Pc/CNT and CNT.

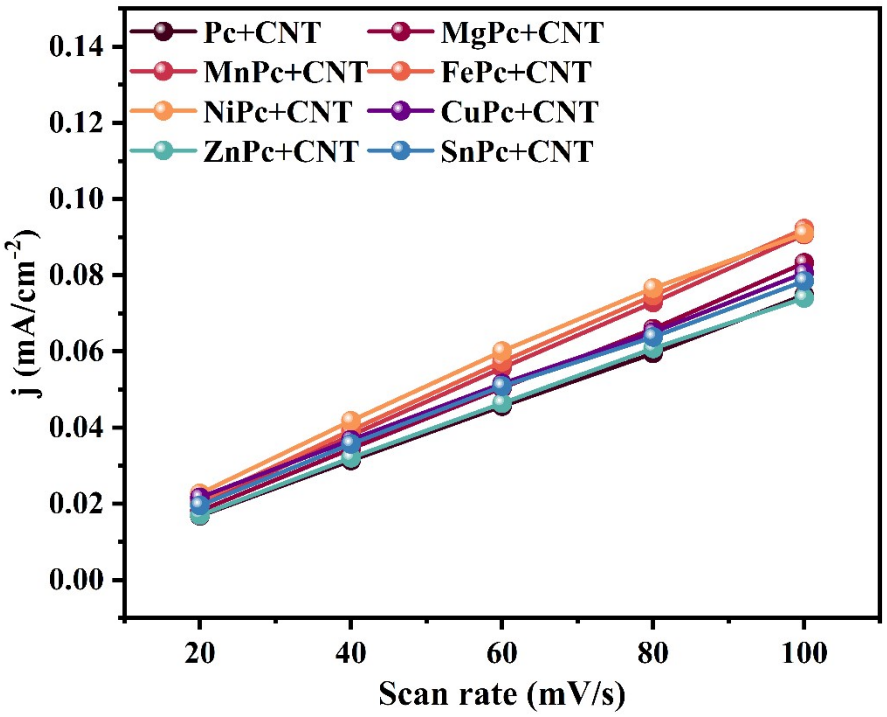

Figure. S12 Electrical double-layer image of MPc/CNT (M = Mg, Mn, Fe, Ni, Cu, Zn, Sn) and Pc/CNT.

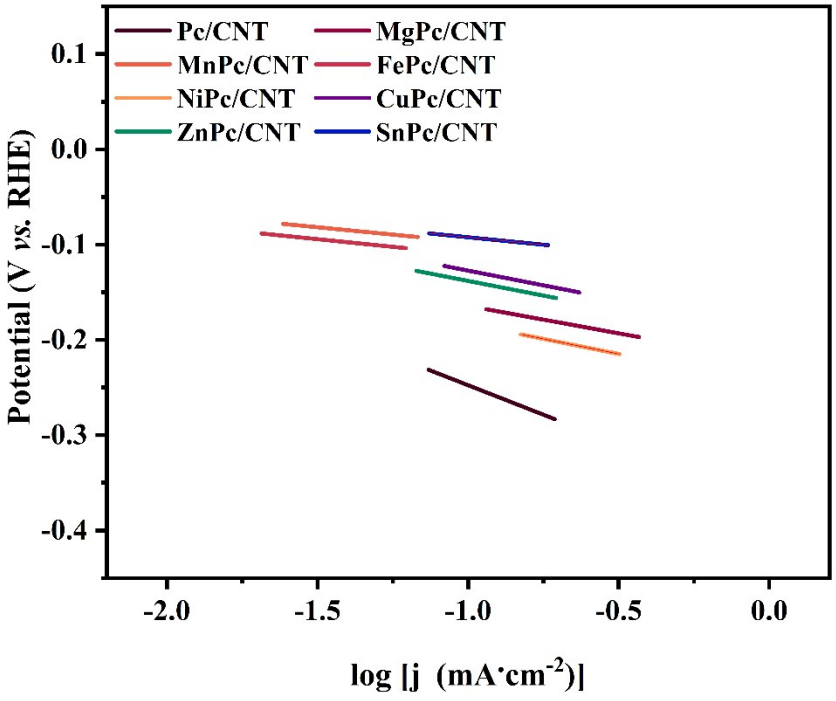

Figure. S13 Tafel image of MPc/CNT (M = Mg, Mn, Fe, Ni, Cu, Zn, Sn) and

Pc/CNT.

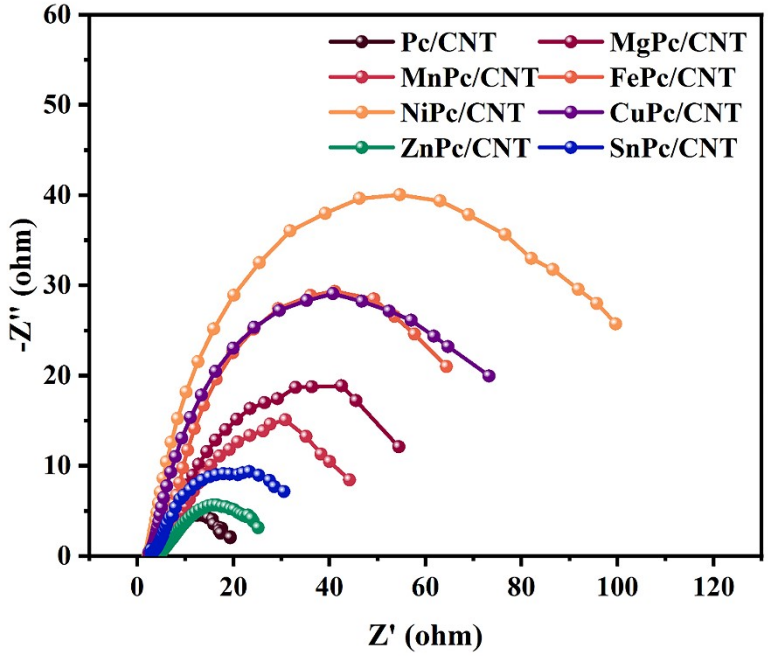

Figure. S14 EIS image of MPc/CNT (M = Mg, Mn, Fe, Ni, Cu, Zn, Sn) and Pc/CNT.

Supplementary Table

Table 1 The C_{dl} data to catalysts.

	C_{dl} mF/cm^2
Pc/CNT	**0.7135**
MgPc/CNT	**0.8825**
MnPc/CNT	**0.8087**
FePc/CNT	**0.8163**
CoPc/CNT	**0.8307**
NiPc/CNT	**0.8827**
CuPc/CNT	**0.7306**
ZnPc/CNT	**0.7205**
SnPc/CNT	**0.7297**
CNT	**0.7105**

Table 2 The Tafel data to catalysts.

	Tafel mV/dec
Pc/CNT	**123.71**
MgPc/CNT	**59.52**
MnPc/CNT	**32.09**
FePc/CNT	**30.87**
CoPc/CNT	**31.78**
NiPc/CNT	**63.29**
CuPc/CNT	**61.74**
ZnPc/CNT	**60.49**
SnPc/CNT	**31.29**
CNT	**125.03**

Table 3 The metal content of catalyst.

	ω %
Mg	**0.544**
Mn	**0.736**
Fe	**0.531**
Co	**0.753**
Ni	**0.832**
Cu	**0.717**
Zn	**0.726**
Sn	**0.642**

Table 4 The TOF data to catalysts.

	TOF s^{-1}
MgPc/CNT	**0.4317**
MnPc/CNT	**0.3999**
FePc/CNT	**0.6096**
CoPc/CNT	**3.7370**
NiPc/CNT	**1.1724**
CuPc/CNT	**0.4053**
ZnPc/CNT	**0.3943**
SnPc/CNT	**1.0446**

Table 5 Comparison of common catalyst properties.

SACs	Potential (V)	j ($mA \cdot cm^{-2}$)	FE_{CO} (%)	TOF(s^{-1})
Co-N_5[11]	**-0.73**	**4.5**	**99.2**	**0.133**
Ni-N_3-C[12]	**-0.65**	**6.64**	**95.6**	**0.396**
ZN SAs/N-C[13]	**-0.65**	**12.7**	**94.7**	**2.275**
ZnO@ZIF-NiZn[14]	**-1**	**34.3**	**98**	**2.602**
Fe-N4[15]	**-0.58**	**4.59**	**94**	**0.453**
Fe-N-CNF[16]	**-0.53**	**4.71**	**94**	**0.862**
Ni/Fe-N-C[17]	**-1**	**23.7**	**98**	**2.134**
Ni-NG[18]	**-1**	**200**	**95**	**0.583**
Ni-N@NPC[19]	**0.67**	**30.96**	**98.44**	**0.785**

Table 6 Bader charge (in |e|) of the M atoms in MPc and the spin state of MPc.

	MgPc	MnPc	FePc	CoPc	NiPc	CuPc	ZnPc	SnPc
Bader charge	**1.62**	**1.39**	**1.14**	**1.05**	**0.89**	**1.17**	**1.18**	**1.24**
Spin state	**0.00**	**3.00**	**2.00**	**1.00**	**0.00**	**1.00**	**0.00**	**0.00**

Table 7 Free energy changes (in eV) of CO_2RR intermediates supported on MPc (M = Mg, Mn, Fe, Co, Ni, Cu, Zn, and Sn).

MPc	* + CO_2	*CO_2	*COOH	*CO	* +CO
MgPc	**0.00**	**0.16**	**2.31**	**0.81**	**0.65**
MnPc	**0.00**	**0.25**	**0.78**	**-0.04**	**0.65**
FePc	**0.00**	**0.22**	**0.71**	**-0.34**	**0.65**

CoPc	**0.00**	**0.21**	**0.42**	**0.26**	**0.65**
NiPc	**0.00**	**0.24**	**2.10**	**0.92**	**0.65**
CuPc	**0.00**	**0.28**	**2.24**	**0.92**	**0.65**
ZnPc	**0.00**	**0.27**	**2.25**	**0.88**	**0.65**
SnPc	**0.00**	**0.34**	**1.56**	**0.98**	**0.65**

References

1. G. Kresse and J. Furthmüller, Physical Review B, 1996, 54, 11169–11186.
2. G. Kresse and J. Furthmüller, Computational Materials Science, 1996, 6, 15-50.
3. G. Kresse and D. Joubert, Physical Review B, 1999, 59, 1758-1775.
4. P. E. Blöchl, Physical Review B, 1994, 50, 17953-17979.
5. J. P. Perdew, K. Burke and M. Ernzerhof, Physical Review Letters, 1996, 77, 3865-3868.
6. S. Grimme, J. Antony, S. Ehrlich, and S. Krieg, The Journal of Chemical Physics, 2010, 132, 154104.
7. S. Grimme, S. Ehrlich, and L. Goerigk, Journal of Computational Chemistry, 2011, 32, 1456-1465.
8. J. K. Nørskov, J. Rossmeisl, A. Logadottir, L. R. K. J. Lindqvist, J. R. Kitchin, T. Bligaard and H. Jonsson, Journal of Physical Chemistry B, 2004, 108, 17886-17892.
9. J. Yin, Z. Yin, J. Jin, M. Sun, B. Huang, H. Lin, Z. Ma, M. Muzzio, M. Shen, C. Yu, H. Zhang, Y. Peng, P. Xi, C. H. Yan and S. Sun, Journal of the American Chemical Society, 2021, 143, 15335-15343.
10. J. H. Montoya, C. Tsai, A. Vojvodic and J. K. Nørskov, ChemSusChem, 2015, 8, 2180-2186.
11. Pan, R. Lin, Y. Chen, S. Liu, W. Zhu, X. Cao, W. Chen, K. Wu, W.-C. Cheong, Y. Wang, L. Zheng, J. Luo, Y. Lin, Y. Liu, C. Liu, J. Li, Q. Lu, X. Chen, D. Wang, Q. Peng, C. Chen and Y. Li, Journal of the American Chemical Society, 2018, 140, 4218-4221.
12. Y. Zhang, L. Jiao, W. Yang, C. Xie and H.-L. Jiang, Angewandte Chemie-International Edition, 2021, 60, 7607-7611.
13. M. Fang, X. Wang, X. Li, Y. Zhu, G. Xiao, J. Feng, X. Jiang, K. Lv, Y. Zhu and W.-F. Lin, Chemcatchem, 2021, 13, 603-609.
14. Y. Hou, Y.-L. Liang, P.-C. Shi, Y.-B. Huang and R. Cao, Applied Catalysis B-Environmental, 2020, 271, 118929.
15. F. Pan, B. Li, E. Sarnello, Y. Fei, X. Feng, Y. Gang, X. Xiang, L. Fang, T. Li, Y. H. Hu, G. Wang and Y. Li, Acs Catalysis, 2020, 10, 10803-10811.
16. Q. Cheng, K. Mao, L. Ma, L. Yang, L. Zou, Z. Zou, Z. Hu and H. Yang, Acs Energy Letters, 2018, 3, 1205-1211.
17. W. Ren, X. Tan, W. Yang, C. Jia, S. Xu, K. Wang, S. C. Smith and C. Zhao, Angewandte Chemie-International Edition, 2019, 58, 6972-6976.

18. K. Jiang, S. Siahrostami, T. Zheng, Y. Hu, S. Hwang, E. Stavitski, Y. Peng, J. Dynes, M. Gangisetty, D. Su, K. Attenkofer and H. Wang, Energy & Environmental Science, 2018, 11, 893-903.
19. H. Wang, M. Li, G. Liu, L. Yang, P. Sun and S. Sun, New Journal of Chemistry, 2021, 45, 1063-1071.